On the effect of "glancing" collisions in the cold atom vacuum standard

Stephen P. Eckel,* Daniel S. Barker, James A. Fedchak, and Julia Scherschligt
Sensor Science Division, National Institute of Standards and Technology, Gaithersburg, Maryland 20899, USA

Jacek Kłos
Joint Quantum Institute, College Park, Maryland 20742, US and
Department of Physics, University of Maryland, College Park, Maryland, 20742, USA

Eite Tiesinga
Joint Quantum Institute, College Park, Maryland 20742, US
Department of Physics, University of Maryland, College Park, Maryland, 20742, USA and
Quantum Measurement Division, National Institute of Standards and Technology, Gaithersburg, Maryland 20899, USA

(Dated: February 21, 2025)

We theoretically investigate the effect of "glancing" collisions on the ultra-high vacuum (UHV) pressure readings of the cold atom vacuum standard (CAVS), based on either ultracold ^{7}Li or ^{87}Rb atoms. Here, glancing collisions are those collisions between ultracold atoms and room-temperature background atoms or molecules in the vacuum that do not impart enough kinetic energy to eject an ultracold atom from its trap. Our model is wholly probabilistic and shows that the number of the ultracold atoms remaining in the trap as a function of time is non-exponential. We update the recent results of a comparison between a traditional pressure standard—a combined flowmeter and dynamic expansion system—to the CAVS [D.S. Barker, *et al.*, *AVS Quantum Science* **5** 035001 (2023)] to reflect the results of our model. We find that the effect of glancing collisions shifts the theoretical predictions of the total loss rate coefficients for ^{7}Li colliding with noble gases or N_2 by up to 0.6 %. Likewise, we find that in the limit of zero trap depth the experimentally extracted loss rate coefficients for ^{87}Rb colliding with noble gases or N_2 shift by as much as 2.2 %.

I. INTRODUCTION

Cold atom vacuum standards measure vacuum pressures by observing the loss rate of cold, "sensor" atoms from a shallow, conservative trap due to collisions with background gases at temperature T and number density n [1–15]. Most collisions impart sufficient energy ΔE such that the total energy E of the sensor atom after the collision is larger than the trap depth W, causing a sensor atom to be ejected from the trap and lost. If all collisions result in loss, then the sensor atom loss is exponential in time with loss rate $\Gamma = Kn$, where K is the collision rate coefficient with SI unit cm^3/s and n with SI unit cm^{-3}. However, some collisions are "glancing": they do not impart enough energy to eject an atom from the trap. These glancing collisions represent an important systematic effect for CAVS-based vacuum pressure measurements.

How to treat systematics due to the glancing collisions has been a matter of discussion in the literature. The simplest means to assess systematics is to assume, as done implicitly in Refs. [9–11, 14–19], (1) that the temperature of the sensor atom cloud T_S is zero, and (2) a sensor atom that has experienced a glancing collision has the same energy as before the collision, i.e., heating due to glancing collisions is ignored. Given the probability that a single collision adds a positive energy less than ΔE to the sensor atom's kinetic energy in the trap, $P_A(\Delta E)$, these two assumptions imply that the atom loss will still be exponential but with rate $\Gamma = Kn[1 - P_A(W)]$. Here, $\Delta E = W$ because under assumptions (1) and (2), the sensors atoms are always assumed to have an energy $E = 0$, as $T_S = 0$, and thus require *at least* an energy W to be ejected from the trap. (See App. A for an explanation of the kinematics and the sign of ΔE.) Various theoretical expressions for $P_A(\Delta E)$ exist in the literature [20]. These will be discussed later in the text.

Estimates show that if ^{87}Rb is used as a sensor atom, $P_A(\Delta E)$ is on the order of 10 % for most collision partners at $T = 300$ K and $\Delta E/k_B \approx W/k_B \sim 1$ mK, where k_B is the Boltzmann constant. For ^{7}Li sensor atoms, $P_A(\Delta E)$ is about an order of magnitude smaller. Reference [12] relaxed the first of these two assumptions and derived a modified form for the observed loss rate for $T_S > 0$. Reference [21] addressed the second of these two assumptions to measure the properties of Rb+Rb collisions. Likewise, Ref. [22] relaxed both assumptions and found that the measured collision rates could be shifted by as much as 3 % for Ar background atoms colliding with ^{87}Rb.

Inspired by the developments of Refs. [12, 21, 22], we construct a comprehensive model to relax both assumptions. Unlike Ref. [22], our model is probabilistic and analytic, which simplifies the fitting of experimental data. Assuming a gas of non-interacting sensor atoms at time $t = 0$, the probability that a sensor atom in the ensemble has an energy less than E is denoted by cumulative distribution function $P_0(T_S, E_c, E)$, where T_S is the initial temperature of the sensor-atom ensemble and E_c is an energy cutoff, such that $P_0(T_S, E_c, E) = 1$ for $E > E_c$. [Throughout this paper, we denote cumulative distribution functions (CDFs) with upper case P, and their corresponding probability density functions (PDFs) with lower case p. The relationship between the two is $P(x) = \int_{-\infty}^{x} dx' \, p(x')$ and $p(x) = dP(x)/dx$ [23].]

* stephen.eckel@nist.gov

In time interval $[0,t]$ with $t>0$, an atom in the ensemble can have experienced none, one, two, etc. collisions with background gas atoms or molecules or have $k=0,\,1,\,2,\,\cdots$ collisional events. The probability for each case satisfies a Poisson distribution $P_k^{(c)}(t)$ with rate Kn. If a sensor atom experiences a single collision after a time t its energy will increase. The probability that a sensor atom has an energy less than E after a single collision is then denoted by $P_{k=1}(T_{\rm S},E_{\rm c},E)$ and can be calculated by noting that $E=E'+\Delta E$ is the sum of independent random variables E' and ΔE, the initial and added kinetic energy, respectively, resulting in the convolution $P_1(T_{\rm S},E_{\rm c},E)=\int dE' p_{\rm A}(E-E')P_0(T_{\rm S},E_{\rm c},E')$ [23], where $p_{\rm A}(\Delta E)={\rm d}P_{\rm A}(\Delta E)/{\rm d}\Delta E$. Likewise, it is possible that the sensor atom has experienced $k>1$ collisions after a time t and we observe that the combined probability $P_{\rm R}(E,t)$ for a sensor atom in the ensemble to have total energy less than E is

$$\begin{aligned} P_{\rm R}(E,t) &= P_0^{(c)}(t)P_0(T_{\rm S},E_{\rm c},E)+P_1^{(c)}(t)P_1(T_{\rm S},E_{\rm c},E) \\ &\quad +P_2^{(c)}(t)P_2(T_{\rm S},E_{\rm c},E)+\cdots, \end{aligned} \tag{1}$$

where $P_k(E)$ are the probabilities that an atom has total energy less than E after $k=0,\,1,\,2,\,\ldots$ collisions. In Sec. II, we calculate the cumulative distribution functions $P_k(T_{\rm S},E_{\rm c},E)$ and show that, under reasonable conditions, the fractional number of sensor atoms remaining in the trap as a function of time $\eta_{\rm S}(t)=P_{\rm R}(E=W,t)$ becomes non-exponential.

A recent comparison by the current authors between cold atom vacuum standards and a classical vacuum metrology apparatus showed uncertainties in pressure measurements approaching 1 % [15], but used the two simplistic assumptions described above to fit for K and the first two terms of the Taylor expansion of $P_{\rm A}(\Delta E)$ in terms of ΔE. At the 1 % level of accuracy, the effect of two glancing collisions per sensor atom within a time $t\lesssim 3/\Gamma$ is important for ^{87}Rb, because $[P_{\rm A}(W)]^2\sim 1$ %. This glancing collision effect was not included in the uncertainty budget of Ref. [15]. In Sec. IV, we correct the recent data of Ref. [15] based on our analytic model. In App. A, we give a brief review of the kinematics, while in App. B, we both review the details of experiment of Ref. [15] and refine the estimate of the temperature of the ^{87}Rb cloud used in Ref. [15].

II. PROBABILISTIC MODEL OF SENSOR-ATOM LOSS

Our probabilistic model of atom loss begins by noting that the ultracold sensor atom clouds are dilute and far away from quantum degeneracy, i.e., the average time between collisions among sensor atoms is much longer than $1/(Kn)$ and thus the sensor-atom cloud is effectively a non-interacting gas of atoms. For the ^{7}Li gases in Ref. [15], the rate of collisions between sensor atoms $K_{\rm S}n_{\rm S}\sim 10^{-6}$ s^{-1} at the maximum possible sensor atom number densities of $n_{\rm S}\sim 10^6$ cm^{-3} and rate coefficient $K_{\rm S}\approx 1.5\times 10^{-12}$ cm^3/s. This rate is much smaller than any measured Γ in the UHV domain by Ref. [15]. For the ^{87}Rb gases in Ref. [15], $K_{\rm S}n_{\rm S}\approx 0.03$ s^{-1}, when averaged over the entire, non-uniform density of the cloud using a peak density of $n_{\rm S}\approx 1.6\times 10^9$ cm^{-3}, a temperature $T_{\rm S}=53(11)$ μK (see App. B), and $K_{\rm S}\sim 1.2\times 10^{-10}$ cm^3/s. This rate is a factor of two smaller than the smallest measured Γ in Ref. [15]. We thus need only to construct a probabilistic loss model for an ensemble of traps, each containing a single sensor atom. An atom has one or more collisions with atoms or molecules in the vacuum before it leaves its trap.

The experimental design of traps for ultracold atoms has a significant impact on the equilibrium or initial $t=0$ probability distribution of the atoms. First, as mentioned before, these traps have a finite depth W but, in addition, in the process of cooling the sensor atoms the experimentalists use what is informally called a "knife" that removes any atom with a motional energy larger than cut-off energy $E_{\rm c}$ that is often significantly lower than W. Moreover, the trapping potential $U(\mathbf{r})$ as function of location $\mathbf{r}$ limits the spatial excursions of the atoms. Assuming that the potential energy of the trap is smallest at $\mathbf{r}=\mathbf{0}$ and that $U(\mathbf{0})=0$, the cumulative distribution function of a sensor atom having an energy less than E is given by

$$P_0(E)\propto\int_0^E {\rm d}E'\rho(E')e^{-E'/k_{\rm B}T_{\rm S}}\,, \tag{2}$$

where $\rho(E)$ is the density of states that depends on $U(\mathbf{r})$. For a separable, power law potential of the form

$$U(x,y,z)=c_1|x|^p+c_2|y|^q+c_3|z|^s\,, \tag{3}$$

where $p,q,s>0$, $|x|$ is the absolute value of real x, and $c_i>0$ for $i=1$, 2, and 3, the density of states obeys [24–26]

$$\rho(E)\propto E^{1/2+1/p+1/q+1/r}\equiv E^{1/2+\delta}\,. \tag{4}$$

Equation (2) can then be evaluated analytically and is

$$P_0(T_{\rm S},E_{\rm c},E) = \frac{\gamma(3/2+\delta,E/k_{\rm B}T_{\rm S})}{\gamma(3/2+\delta,E_{\rm c}/k_{\rm B}T_{\rm S})} \tag{5}$$

when $E<E_{\rm c}$ and 1 otherwise. Here, $\gamma(a,x)=\int_0^x y^{a-1}e^{-y}\,dy$ is the incomplete gamma function.

For a magneto-optical trap (MOT) with its linear trapping force and thus quadratic potential along all three spatial dimensions, $\delta=3/2$. For a magnetic quadrupole trap with constant trapping force and thus a linear potential along all three spatial axes, $\delta=3$. For a constant or box potential, $\delta=0$. The sensor-atom clouds created in Ref. [15] were last in thermal equilibrium in a MOT, and thus we anticipate that $\delta=3/2$. Subsequent measurements, described in App. B, confirm this.

For time $t>0$, collisions between a sensor atom and background atoms and molecules occur at random times with a timescale of $1/(Kn)$. The cumulative distribution function of collision times is then Poisson and

$$P_k^{(c)}(t)=\frac{1}{\Gamma(k+1)}(Knt)^k e^{-Knt}\,, \tag{6}$$

where $\Gamma(z)$ is the Gamma function [23].

System	α_1/k_B (mK^{-1})	α_2/k_B^2 (mK^{-2})
^{87}Rb-H_2	0.037	−0.002
^{87}Rb-He	0.014	−0.00028
^{87}Rb-Ne	0.053	−0.003
^{87}Rb-N_2	0.076	0.0068
^{87}Rb-Ar	0.079	−0.0072
^{87}Rb-Kr	0.11	−0.014
^{87}Rb-Xe	0.14	−0.024

TABLE I. Values of coefficients α_i for ^{87}Rb sensor atoms with $i = 1$ and 2 in Eq. (10) derived from the theory of Ref. [14]. No uncertainties are presented as the table is only meant to indicate relative sizes of the α_i. Values for α_i with $i > 2$ are currently unknown and assumed to be zero in our simulations.

The cumulative distribution function $P_0(E,T_S,E_c)$ is defined in Eq. (5) and, more generally, $P_k(E,T_S,E_c)$ are the cumulative distribution functions that an atom has total energy less than E after $k = 0, 1, 2, \ldots$ collisions. We can derive $P_k(E,T_S,E_c)$ recursively. After the k-th collision, $P_k(E,T_S,E_c)$ is given by the convolution of the probability density $p_A(\Delta E)$ that the collision adds energy $\Delta E > 0$ to the sensor atom and the cumulative distribution $P_{k-1}(E',T_S,E_c)$ such that $E = E' + \Delta E$. Following App. A we realize that nearly all collisions add energy to the sensor atoms and assume $p_A(\Delta E) = 0$ for $\Delta E < 0$. Consequently,

$$P_k(T_S,E_c,E) = \int_0^\infty dE' p_A(E-E') P_{k-1}(T_S,E_c,E') . \quad (7)$$

The probability density function $p_A(\Delta E)$ is found by noting that

$$\int_0^{\Delta E} d\varepsilon p_A(\varepsilon) \equiv P_A(\Delta E) \quad \text{or} \quad p_A(\Delta E) = \frac{dP_A(\Delta E)}{d(\Delta E)} \quad (8)$$

with dimensionless cumulative distribution function $P_A(\Delta E)$ defined previously in the literature as [9–14, 21, 27, 28]

$$P_A(\Delta E) = \frac{1}{K} \left\langle \int_0^{\theta_c(\Delta E)} d\theta \int_0^{2\pi} d\varphi \, v_{rel} \frac{d\sigma}{d\Omega} \right\rangle , \quad (9)$$

where $d\sigma/d\Omega$ is the elastic differential cross section, v_{rel} is the relative collision velocity, the integration over the polar angle θ is limited to angles smaller than the ΔE-dependent cutoff $\theta_c(\Delta E)$, $\langle \cdots \rangle$ represents a thermal average over a Boltzmann distribution at effective temperature $T_{eff} = mT/(m+M) < T$, where m is the mass of a sensor atom and M is the mass of a background atom or molecule. Finally, $K = \langle v_{rel}\sigma \rangle$ with cross section σ is the collision rate coefficient or more precisely the thermalized elastic rate coefficient at temperature T_{eff}. The function $P_A(\Delta E) \in [0,1]$ is a monotonically increasing function of ΔE. Moreover, as typical trap depths and thus ΔE are of order $k_B \times 1$ mK orders of magnitude smaller than $k_B T_{eff}$, we parameterize

$$P_A(\Delta E) = \alpha_1 \Delta E + \alpha_2 (\Delta E)^2 + \cdots \quad (10)$$

and

$$p_A(\Delta E) = \alpha_1 + 2\alpha_2 \Delta E + \cdots \quad (11)$$

for $\Delta E \geq 0$ and zero otherwise.

The collisional quantities α_i in Eq. (10) have been computed from first principles in Ref. [14]. As will be seen in Sec. IV, only terms up to α_2 in this equation are required. We use $\alpha_1 = a_{gl}/K$ and $\alpha_2 = b_{gl}/K$ with the coefficients K, a_{gl}, b_{gl} taken from Ref. [14]. For ^{87}Rb, the relevant α_i are given in Table I and we realize that $\alpha_2 W^2 \ll \alpha_1 W \ll 1$ for $W/k_B \approx 1$ mK. For ^{7}Li sensor atoms these inequalities also hold. An alternative choice from Refs. [10–12, 21, 28] results in $\alpha_j = \beta_j/(U_d)^j$, where $U_d = 4\pi\hbar^2/[m(K/\langle v \rangle)]$ is the "diffractive collision energy scale", the median energy exchanged in the collision with mean velocity $\langle v \rangle = \sqrt{k_B T/2M}$ [10, 29]. Typically, $U_d \gg W$. The dimensionless coefficients β_j are argued to be independent of the collision pair and are given in Table 1 of Ref. [10].

It reasonable to assume that $p_A(\Delta E)$ and $P_A(\Delta E)$ are independent of the initial collision energy as long as $\Delta E \gg k_B T_S$, with sensor atoms essentially at rest, and index k limited to only a few collisions. As discussed in Refs. [15–17], the change in $P_A(\Delta E)$ due to a finite initial velocity of the ultracold atoms is of the order of $(m/\mu)(T_S/T) \sim 10^{-5}$, where μ is the reduced mass of the collision partners. This change is negligible at our level of accuracy.

The probabilities $P_k(T_S,E_c,E)$ can be evaluated using (7), (10), (8), and (5). The chapter on the confluent hypergeometric function found in Ref. [30] is particularly useful, after we express the incomplete gamma function in terms of the Kummer's confluent hypergeometric function. After some thought, we obtain

$$P_1(T_S,E_c,E) = \sum_{i=1}^{\infty} \alpha_i (k_B T_S)^i \begin{cases} \mathscr{M}_i\left(\frac{3}{2}+\delta, \frac{E_c}{k_B T_S}, \frac{E}{k_B T_S}\right) & E < E_c \\ \sum_{k=0}^{i} \binom{i}{k} \left(\frac{E-E_c}{k_B T_S}\right)^k \mathscr{M}_{i-k}\left(\frac{3}{2}+\delta, \frac{E_c}{k_B T_S}, \frac{E_c}{k_B T_S}\right) & E \geq E_c \end{cases} , \quad (12)$$

where $\binom{i}{k}$ is the binomial coefficient, dimensionless function

$$\mathscr{M}_i(a,x_c,x) \equiv i \int_0^x d\varepsilon (x-\varepsilon)^{i-1} \frac{\gamma(a,\varepsilon)}{\gamma(a,x_c)} \quad (13)$$

$$= x^i \left(\frac{x}{x_c}\right)^a \frac{\Gamma(i+1)\mathbf{M}(a,a+i+1,-x)}{\mathbf{M}(a,a+1,-x_c)} , \quad (14)$$

and Kummer's (regularized) confluent hypergeometric function $\mathbf{M}(a,b,z)$ is defined in Eqs. (13.2.E3) and (13.2.E4) of

Ref. [30]. In the derivation of Eq. (14), we have also used Eqs. (13.6.E5) and (13.4.E2) of this reference. We observe that Eq. (14) allows us to define $\mathscr{M}_i(a,x_c,x)$ for $i=0$ and realize that $\mathscr{M}_0(a,x_c,x_c)=1$. Finally, note that

$$\mathscr{M}_i(a,x_c,x_c) \to x_c^i\left(1-i\frac{a}{x_c}+O(1/x_c^2)\right) \tag{15}$$

for $x_c \to +\infty$ based on Eq. (13.7.E2) of Ref. [30]. Consequently, focusing on $E \approx W$ and realizing that $k_B T_S \ll E_c < W$, we have

$$P_1(T_S,E_c,E) \to \sum_{i=1}^{\infty}\alpha_i\left[\sum_{k=0}^{i}\binom{i}{k}(E-E_c)^k E_c^{i-k}\right. \tag{16}$$
$$\left.-(3/2+\delta)k_B T_S\sum_{k=0}^{i}\binom{i}{k}(i-k)(E-E_c)^k E_c^{i-k-1}\right]$$
$$= \sum_{i=1}^{\infty}\alpha_i E^i\left[1-(3/2+\delta)i\frac{k_B T_S}{E}\right] \tag{17}$$
$$= P_A(E)-(3/2+\delta)k_B T_S p_A(E), \tag{18}$$

where in the formula in square brackets we recognize the binomial formula and its derivative.

Next, we derive

$$P_2(T_S,E_c,E) = \sum_{j=1}^{\infty}\sum_{i=1}^{\infty}\alpha_j\alpha_i(k_B T_S)^{i+j}\frac{\Gamma(i+1)\Gamma(j+1)}{\Gamma(i+j+1)}\begin{cases}\mathscr{M}_{i+j}\left(\frac{3}{2}+\delta,\frac{E_c}{k_B T_S},\frac{E}{k_B T_S}\right) & E<E_c\\ \sum_{k=0}^{i+j}\binom{i+j}{k}\left(\frac{E-E_c}{k_B T_S}\right)^k\mathscr{M}_{i+j-k}\left(\frac{3}{2}+\delta,\frac{E_c}{k_B T_S},\frac{E_c}{k_B T_S}\right) & E\geq E_c\end{cases} \tag{19}$$

again using Eq. (13.4.E2) of Ref. [30]. Again focusing on $E \approx W$ and realizing that $k_B T_S \ll E_c < W$, we have

$$P_2(T_S,E_c,E) \to \sum_{j=1}^{\infty}\sum_{i=1}^{\infty}\alpha_j\alpha_i\frac{\Gamma(i+1)\Gamma(j+1)}{\Gamma(i+j+1)}E^{i+j} = \frac{1}{2}\alpha_1^2E^2+\frac{2}{3}\alpha_1\alpha_2E^3+\cdots \tag{20}$$

as we again recognized a binomial formula in $E-E_c$ and E_c. We also observe that $P_2(T_S,E_c,E) \approx [P_A(E)]^2/2$.

For completeness, we have

$$P_3(T_S,E_c,E) = \sum_{l=1}^{\infty}\sum_{j=1}^{\infty}\sum_{i=1}^{\infty}\alpha_l\alpha_j\alpha_i(k_B T_S)^{i+j+l} \tag{21}$$
$$\times\frac{\Gamma(i+1)\Gamma(j+1)\Gamma(l+1)}{\Gamma(i+j+l+1)}\begin{cases}\mathscr{M}_{i+j+l}\left(\frac{3}{2}+\delta,\frac{E_c}{k_B T_S},\frac{E}{k_B T_S}\right) & E<E_c\\ \sum_{k=0}^{i+j+l}\binom{i+j+l}{k}\left(\frac{E-E_c}{k_B T_S}\right)^k\mathscr{M}_{i+j+l-k}\left(\frac{3}{2}+\delta,\frac{E_c}{k_B T_S},\frac{E_c}{k_B T_S}\right) & E\geq E_c\end{cases}$$

The expressions for $P_k(T_S,E_c,E)$ for $k=4,5,\cdots$ follow by inspection from Eqs. (12), (19), and (21). For $k_B T_S \ll E_c < E$ we then derive

$$P_k(T_S,E_c,E) \approx \frac{1}{\Gamma(k+1)}\alpha_1^k E^k\left(1-k(3/2+\delta)\frac{k_B T}{E}\right) \tag{22}$$
$$+\frac{2k}{\Gamma(k+2)}\alpha_1^{k-1}\alpha_2E^{k+1}\left(1-(k+1)(3/2+\delta)\frac{k_B T}{E}\right)$$

for $k=0,1,\ldots$ leading to an approximate analytical expression for the time evolution of the cumulative distribution function for an atom in the ensemble to have total energy less than E that is given by

$$P_R^{\rm approx}(E,t) = e^{-Knt}\left\{I_0(2y)-(3/2+\delta)\frac{k_B T}{E}yI_1(2y)\right. \tag{23}$$
$$+2\frac{\alpha_2 E}{\alpha_1}\left(1-2(3/2+\delta)\frac{k_B T}{E}\right)I_2(2y)$$
$$\left.-2(3/2+\delta)\frac{\alpha_2 k_B T}{\alpha_1}yI_3(2y)\right\}$$

with $y=\sqrt{\alpha_1 EKnt}$ and is thus non-exponential in time. Here, $I_n(z)$ is the modified Bessel function of the first kind, $I_n(z) \to (z/2)^n/\Gamma(n+1)$ for $z\to 0$, and $I_n(z) \to e^z/\sqrt{2\pi z}$ for $z\to\infty$. Equations (22) and (23) form two of the main analytical results of this article.

Two further, less accurate approximations for the cumulative distribution function $P_R(E,t)$ are relevant to compare with

previous work. We can find these approximations by rewriting Eqs. (1) and (6) in the equivalent cumulant form

$$P_{\rm R}(E,t) = P_0 e^{-(1-P_1/P_0)Knt+(P_0P_2-P_1^2)(Knt)^2/(2P_0^2)+O(t^3)} \quad (24)$$

as can be verified from a Taylor expansion in t. Here, we have suppressed the three arguments of the cumulative distribution functions $P_k(T_{\rm S},E_{\rm c},E)$ for clarity. The terms proportional to t^2, t^3, etc in the exponential lead to non-exponential behavior. If only assumption (2) holds, *i.e.* glancing collisions do not change the energy of an atom, then the cumulative distribution function that an atom survives i uncorrelated collisions is equal to the probability that an atom survives one collision raised to the ith power. This corresponds to the choice $P_k(T_{\rm S},E_{\rm c},E) = [P_1(T_{\rm S},E_{\rm c},E)]^k$ for $k = 0,1,2,\ldots$ and only the term linear in t in Eq. (24) survives leading to

$$P_{\rm R}^{(1)}(E,t) = e^{-[1-P_1(T_{\rm S},E_{\rm c},E)]Knt}, \quad (25)$$

equivalent to the result of Ref. [12]. When both assumptions hold, we have $P_k(T_{\rm S},E_{\rm c},E) = [P_{\rm A}(E)]^k$ for $k = 0,1,2,\ldots$ and

$$P_{\rm R}^{(\rm A)}(E,t) = e^{-[1-P_{\rm A}(E)]Knt} \quad (26)$$

used in Refs. [11, 13–15], respectively. With Eq. (23), we have shown that the exponential time evolutions in Eqs. (25) and (26) are only valid up to first order in $P_{\rm A}(E)$ or, more precisely, up to first order in $\alpha_1 E$.

Finally, we note that the fraction of remaining trapped sensor atoms in the ensemble $\eta_{\rm S}(t)$ is given by $\eta_{\rm S}(t) = P_{\rm R}(E = W,t)$ [31]. Inspection, remembering that $E_{\rm c} \le W$, shows that $\eta_{\rm S}(t=0) = 1$. For future use, we define a measure of non-exponential behavior by

$$\Xi(W,t) = \left|P_2(T_{\rm S},E_{\rm c},W) - [P_1(T_{\rm S},E_{\rm c},W)]^2\right| Knt \quad (27)$$

based on the ratio of the t^2 and t terms in Eq. (24), where we have used that $P_0(T_{\rm S},E_{\rm c},W) = 1$ and $P_1(T_{\rm S},E_{\rm c},W) \ll 1$ for our sensor atoms.

III. VISUALIZATION OF THE PROBABILISTIC MODEL

Figure 1(a) shows the exact and approximate cumulative distribution functions $P_k(T_{\rm S},E_{\rm c},E)$ scaled by $(\alpha_1 E)^k$ for $k =$ 1, 2 and 3 as functions of E for ^{87}Rb sensor atoms and a Xe background gas using α_1 and α_2 derived from data in Ref. [14], reproduced in our Table III, with parameters $\delta = 3/2$, $E_{\rm c}/k_{\rm B} = 0.2$ mK and $T_{\rm S} = 53$ μK that are motivated by the experiments of Ref. [15] and discussed in App. B. For the largest E shown in the figure, $P_{\rm A}(E) \approx \alpha_1 E \approx 0.2$. We find that, for $E \gg E_{\rm c}$ and all three k, the approximate expression in Eq. (22) approaches the exact expression as expected. Moreover, $P_k(T_{\rm S},E_{\rm c},E)/[P_A(T_{\rm S},E_{\rm c},E)]^k < 1$ for all k and E shown, representing a breakdown of the approximation $P_k(T_{\rm S},E_{\rm c},E) = [P_{\rm A}(E)]^k$ and, consequently, assumptions (1) and (2) described in the introduction.

Figure 1(b) shows $P_{\rm R}(E,t)$, computed from Eq. (1) and our exact expressions for $P_k(T_{\rm S},E_{\rm c},E)$, as functions of E for various hold times t. As in Ref. [21], the curves have a non-continuous derivative at $E = E_{\rm c}$. For $E < E_{\rm c}$, $P_{\rm R}(t,E)$ is mostly determined by the initial cumulative distribution $P_0(T_{\rm S},E_{\rm c},E)$ of atoms in the trap and the probability with time that these atoms have not undergone a collision $p_0^{(c)}(t)$. For $E > E_{\rm c}$, $P_{\rm R}(t,E)$ is independent of E at $t = 0$, indicating no population at these total energies, while for $t > 0$, it acquires an increasing positive slope $dP_{\rm R}(t,E)/dE$ with t, indicating the build up of hotter atoms that have experienced one or more glancing collisions.

The exact remaining fraction of atoms $\eta_{\rm S}(W,t) = P_{\rm R}(W,t)$ as well as several approximations are shown in Fig. 1(c) with $W = 1.5940(2)$ mK and other system parameters as in panels (a) and (b). The exact curve for $\eta_{\rm S}(W,t)$ lies significantly above the exponential loss curve e^{-Knt} of the "ideal" CAVS in the limit $W \to 0$ and lies only slightly below the exponential loss curve of Eq. (25). The non-exponential prediction of Eq. (23) is nearly indistinguishable from the exact result (1), with about a 1.5 % error at $Knt = 6$.

To further validate our analytical calculations, we perform Monte-Carlo simulations of sensor atom loss. The simulations begin at $t = 0$ with 10^6 sensor atoms at initial energies chosen at random according to $P_0(T_{\rm S},E_{\rm c},E)$ in Eq. (5). For each time step $\Delta t = 0.005 \times (1/Kn)$, chosen such that $Kn\Delta t \ll 1$, a random number in the interval [0,1) is chosen for each atom and if that number is smaller than $Kn\Delta t$, then the sensor atom undergoes a collision with a background gas molecule [32]. For sensor atoms undergoing collisions, a random energy ΔE according to the probability density in Eq. (10) is chosen and is added to the sensor atom's current energy. If a sensor atom's new energy is larger than W, the sensor atom is ejected, *i.e.* removed from the ensemble of sensor atoms in the Monte-Carlo simulations. Cumulative distribution functions $P_k^{(\rm MC)}(T_{\rm S},E_{\rm c},E)$, $P_{\rm R}^{(\rm MC)}(E,t)$, and $\eta_{\rm S}^{(\rm MC)}(W,t)$ for the Monte-Carlo simulations are then constructed. The Monte Carlo simulations and our exact results agree; *i.e.,* the curves for the system parameters used in Fig. 1 can not be distinguished on the scales of the three panels in the figure.

IV. EFFECT ON THE RECENT COMPARISON BETWEEN CLASSICAL AND QUANTUM STANDARDS

Decay curves $\eta_{\rm S}(t)$ in the experiments of Ref. [15] were measured for both ^{7}Li and ^{87}Rb sensor atoms colliding with near-room-temperature $X =$ He, Ne, N_2, Ar, Kr, and Xe background gases introduced into the CAVSs at a known number density n. The time evolution of the decay curves was then fit to an exponential with loss rate Γ, which was assumed to be of the form $\Gamma = Ln = Kn[1 - P_{\rm A}(W)]$ with $P_{\rm A}(W) = (a_{\rm gl}W - b_{\rm gl}W^2)/K$. This form for Γ is only valid under assumptions (1) and (2), described in the introduction.

Let us first consider the effect of violating these assumptions on the ^{7}Li-X collision data, which were taken at trap depth $W = k_{\rm B} \times 0.95(14)$ mK, leading to $\alpha_1 W \ll 1$ as the α_1 for ^{7}Li are two orders of magnitude smaller than those for ^{87}Rb sensor atoms. The measured exponential decay rates Γ as functions of n were fit assuming $\Gamma = Ln$ to extract an ob-

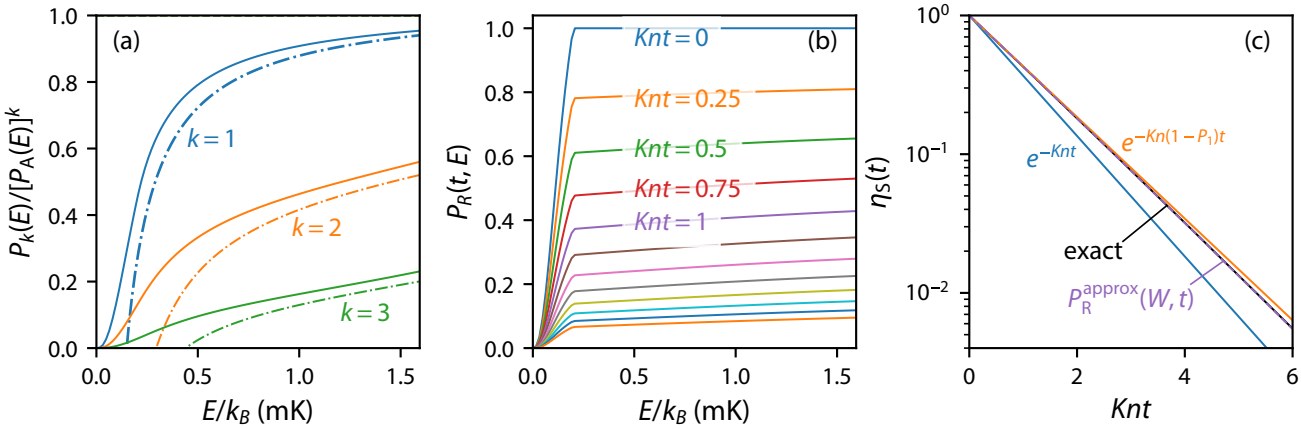

FIG. 1. (a) Exact and approximate scaled cumulative distribution functions $P_k(T_S,E_c,E)/[P_A(E)]^k$ for ^{87}Rb sensor atoms having an energy less than E after $k=1,2,3$ collisions with Xe background gas atoms in blue, orange, and green, respectively. We use the $P_A(\Delta E)$ from Ref. [14] and assume $\delta=3/2$, T_S=53 μK, and $E_c/k_B=0.2$ mK. Solid curves are based on the exact expressions in Eqs. (12), (19), and (21). Dot-dashed curves are based on Eq. (22) extrapolated to $E=0$. (b) Exact cumulative distribution function $P_R(E,t)$ of ^{87}Rb sensor atoms as functions of E at several hold times t based on Eq. (1) using the exact expressions for $P_k(T_S,E_c,E)$. From top to bottom colors encode $Knt=0$ to 2.5 in steps of 0.25. System parameters are the same as those in panel (a). (c) Fractional remaining sensor-atom number $\eta_S(t)=P_R(W,t)$ as functions of Knt with trap depth $W=1.5940$ mK and other system parameters as in panel (a). The solid black curve corresponds to Eq. (1) with the exact expressions for $P_k(T_S,E_c,E)$. The approximation in Eq. (23) is shown as the dashed purple curve. The solid orange curve shows the approximate prediction of Eq. (25). Finally, the solid blue curve shows $\eta_S(t)=e^{-Knt}$ for the "ideal" CAVS, where $W\to 0$.

served rate coefficient L. The fitted L was then compared to the predicted value obtained with quantum mechanical scattering calculations of Ref. [14]. Both theory and experiment relied on assumptions (1) and (2). We thus need to correct the theoretical predictions of L given the finite T_S and characterize potential systematic shifts due to non-exponential decay on the extracted L for ^{7}Li.

To update the theoretical predictions of L, we need an accurate estimate of the temperature T_S for ^{7}Li. A convenient value of $T_S=0.1$ mK was used in Ref. [15], which was not necessarily reflective of the actual temperature. In fact, T_S is not well known. Here, we take a much larger ^{7}Li temperature of $T_S=0.75$ mK from a temperature measurement of such atoms in a MOT in a similar apparatus [33]. We conservatively assume a standard uncertainty of 0.25 mK and observe that $k_BT_S\approx W$. We also take $E_c=W$, and, since the last time the cloud was in thermal equilibrium was in the MOT, we have $\delta=3/2$.

Next, we realize that for the special case $E_c=W=k_BT_S$ and $\delta=3/2$ the cumulative distribution functions $P_k(T_S,E_c,W)$ are

$$P_1(W/k_B,W,W) = \frac{11-4e}{2e-5}\alpha_1 W+O(W^2) \quad (28)$$
$$= 0.290\cdots\alpha_1 W+O(W^2)$$

and

$$P_2(W/k_B,W,W) = \frac{7e-19}{2e-5}(\alpha_1 W)^2+O(W^3) \quad (29)$$
$$= 0.0640\cdots(\alpha_1 W)^2+O(W^3).$$

Equation (28) implies that with $k_BT_S\approx E_c=W$, as in our ^{7}Li experiments, $P_1(T_S,W,W)$ is about three times smaller than $P_A(W)$. This can be compared to $P_1(T_S,E_c,W)=P_A(W)$ when $k_BT_S\ll E_c<W$ analyzed in the previous section. Thus, glancing collisions are less of a concern than assumed in Ref. [15]. Physically, because $k_BT_S\approx W$, it is easier for ^{7}Li atoms to be ejected from the trap.

System	L (thr) (10^{-9}cm^3/s)	L (exp) (10^{-9}cm^3/s)	$E_n(L)$
^{7}Li-^{4}He	1.66(4)	1.72(3)	0.63
^{7}Li-Ne	1.55(14)	1.634(16)	0.28
^{7}Li-N_2	2.65(2)	2.67(3)	0.33
^{7}Li-Ar	2.34(1)	2.38(2)	0.95
^{7}Li-Kr	2.150(7)	2.20(3)	0.65
^{7}Li-Xe	2.25(2)	2.22(3)	−0.45

TABLE II. Theoretical (thr) and updated experimentally (exp) determined loss rate coefficients L for various natural abundance gases colliding with ultracold ^{7}Li sensor atoms. The theoretical values are based on the exponential time evolution in Eq. (25) with $T_S=0.75(25)$ mK, $E_c=W=k_B\times 0.95(14)$ mK, and K, a_{gl} and b_{gl} from Ref. [14]. The last column shows the degree of equivalence $E_n(L)=(L_{exp}-L_{thr})/[2u(L_{exp}-L_{thr})]$. All uncertainties are one-standard deviation $k=1$ uncertainties.

Secondly, our measure for non-exponential behavior $\Xi(W,t)=|P_2-P_1^2|(Knt)\approx 0.02(\alpha_1 W)^2 Knt$ is at most 10^{-5} for all background gases at the largest $Knt=4$ measured in Ref. [15]. Consequently, at our level of accuracy for extracting loss rates Γ for ^{7}Li, contributions from non-exponential decay can be neglected and the rate coefficient $L=K[1-P_1(T_S,E_c,W)]$ with $P_1(T_S,E_c,W)$ from Eq. (28) can be used. Because $0<P_1(T_S,E_c,W)<P_A(W)$, the theoretically predicted values for L are larger than those in Ref. [15]. Moreover, the contribution to the uncertainty of L from W is re-

duced compared to that in Ref. [15]. The updated predictions for L, shown in Table II, are now in better agreement with their experimental counterparts, with the theoretical and experimental values agreeing at two standard deviations ($k = 2$).

An updated uncertainty budget for ^{7}Li-Ar and the change in the theoretical predictions of L from Ref. [15] are shown in the supplemental material, Tables S1 and S2, respectively [34]. The maximum change in L from Ref. [15] is 0.64 % for ^{7}Li+Xe. In fact, for all background gases the change in L is less than our updated corresponding theoretical uncertainty.

The situation is more complicated for ^{87}Rb sensor atoms. Once again, we require a better estimate of the sensor-atom temperature T_S. It is now obtained by measuring the energy distribution of the ^{87}Rb atoms in the quadrupole trap as in Ref. [21] and described in App. B. We find $T_S = 53(12)$ μK ensuring that we are in the limit $k_B T \ll E_c < W$ studied in Sec. II.

In Ref. [15], exponential decay was assumed for the loss of ^{87}Rb sensor-atoms. For $k_B T \ll E_c < W$, the measure of non-exponential behavior $\Xi(W,t) \approx 0.50(\alpha_1 W)^2 Knt$ is largest for a Xe background gas at $\Xi(W,t) = 0.028$ using the longest experimental hold time. This value is comparable to the fractional standard statistical uncertainty $u(\Gamma)/\Gamma$ for the decay rates Γ found from exponential fits to $\eta_S(t)$ versus t. Thus, we refit the data of Ref. [15] to account for non-exponential decay.

For our fit, let us first consider the exact solution in Eq. (1) with the substitutions of $\eta_S(t) = \eta_0 P_R(W,t)$ and $\Gamma_0 = Kn$, which yields

$$\eta_S(t) = \eta_0 e^{-\Gamma_0 t}\left[1 + P_1(\Gamma_0 t) + \frac{1}{2}P_2(\Gamma_0 t)^2 + \frac{1}{6}P_3(\Gamma_0 t)^3 + \cdots\right]. \tag{30}$$

with probabilities $P_k(\cdot,\cdot,\cdot)$ evaluated at $E = W$. One immediate question arises: how many $P_k(T_S, E_c, W)$ must be included given our measurement uncertainties in $\eta_S(t)$? Using a second convenient substitution of $\Gamma_i = Kn\alpha_i = \Gamma_0\alpha_i$ for $i = 1, 2, \ldots$ together with our approximate expression for $P_k(T_S, E_c, W)$ in Eq. (22), we find

$$\eta_S(t) \approx e^{-\Gamma_0 t}\left\{1 + \sum_{i=1}^{2}\Gamma_i W^i\left(1 - i(3/2+\delta)\frac{kT_S}{W}\right)t + \left[\frac{1}{4}(\Gamma_1 W)^2 + \frac{1}{3}\Gamma_1\Gamma_2 W^2\right]t^2 + \frac{1}{36}(\Gamma_1 W)^3 t^3 + \cdots\right\}. \tag{31}$$

Thus, we observe that the dominant coefficient for each t^k in the braces $\{\cdots\}$ is $(\Gamma_1 W)^k/[\Gamma(k+1)]^2$. For the data of Ref. [15], the maximum W for which data was taken is $W/k_B = 1.6$ mK and the maximum t was approximately $3/\Gamma_0$. At $t = 3/\Gamma_0$, the measured relative uncertainty $u(\eta_S(t))/\eta_S(t) \gtrsim \varepsilon \equiv 0.05$. We then demand that $(3\Gamma_1 W/\Gamma_0)^k/[\Gamma(k+1)]^2 < 0.01\varepsilon$ to ensure convergence of the series in Eq. (30). Using the theoretical prediction for ^{87}Rb-Xe of Ref. [14], which has the largest Γ_1 of all studied background gases, this requirement demands computing terms up to and including $k = 4$.

The data of Ref. [15] is further complicated by apparent two-body losses. We thus fit the normalized ^{87}Rb atom number $\eta_S(W,t)$ as a function of t and W for given T_S, E_c, and background gas number density n to the numerical solution of

$$\frac{d\eta_S}{dt} = -\Gamma(W,t)\eta_S - \beta(W)\eta_S^2, \tag{32}$$

with $\eta_S(t=0) = \eta_0$, where the trap depth and time dependent $\Gamma(W,t)$ is

$$\Gamma(W,t) = -\frac{d\log P_R(W,t)}{dt} = -\frac{1 + \sum_{i=1}^{4} P_k t^{k-1}/\Gamma(k)}{1 + \sum_{i=1}^{4} P_k t^k/\Gamma(k+1)} \tag{33}$$

and the two-body loss parameter $\beta(W) = \beta_0 + \beta_1 W$. We have verified that the numerical solution of Eq. (32) using the second equality of Eq. (33) reproduces Eq. (30) to better than 0.0001ε, where $\varepsilon = 0.05$ as before.

For each value of n, the authors of Ref. [15] measured time traces $\eta_S(W,t)$ between $t = 0$ and $t \approx 4/\Gamma_0$ for seven W between $k_B \times 0.4$ mK and $k_B \times 1.6$ mK. The sensor atom temperature and cutoff energy are fixed at $T_S = 53(12)$ μK and $E_c = k_B \times 0.1993(2)$ mK, respectively. Moreover, we assume $\delta = 3/2$. The quality of the experimental data determines the number of Γ_i included in the fit. We use Γ_i for $i = 1, \cdots, i_{max}$, where i_{max} is the first value of i that satisfies $\Gamma_{i_{max}} < 2u(\Gamma_{i_{max}})$ and $u(\Gamma_i)$ is the statistical standard uncertainty in Γ_i. Consequently, for ^{87}Rb-He the adjusted parameters are η_0, Γ_0, Γ_1, β_0, and β_1. For all others systems, Γ_2 is the sixth adjusted parameter. We propagated the 20 % uncertainty of T_S through the fits by determining $d\Gamma_i/dT_S$ for $i = 0, \cdots, i_{max}$. The < 0.1 % uncertainties of E_c and W are negligible contributions to our total uncertainty. The fitted $\beta(W) > 0$ at a 2-σ ($k = 2$) uncertainty for 33 % of our time traces, possibly indicating the presence of two body collisional induced loss. For the remaining fits, $\beta(W)$ is consistent with zero at 2-σ.

By construction for each background gas, fitted quantities Γ_i with $i = 0, \cdots, i_{max}$ should only be proportional to the background gas number density n. We, however, observe offsets as function of n and thus obtain rate coefficients K and glancing collision rates a_{gl} and b_{gl} for the roughly 10 values of n between 4×10^7 cm^{-3} and 4×10^9 cm^{-3} using

$$\begin{aligned}\Gamma_0 &= Kn + \Gamma_{0,base},\\ \Gamma_1 &= a_{gl} n + \Gamma_{1,base},\\ \Gamma_2 &= b_{gl} n + \Gamma_{2,base}.\end{aligned} \tag{34}$$

with offsets $\Gamma_{i,base}$ as two additional adjusted parameters for ^{87}Rb-He and three additional adjusted parameters for all others background gases. In these second, linear fits, we have accounted for the uncertainties of and covariances among the two or three Γ_i obtained by fitting the time traces as well as the roughly 0.3 % relative uncertainty in n. Rate $\Gamma_{0,base}$ is 0.027(6) s^{-1} independent of the background gas species. $\Gamma_{1,base}$ and $\Gamma_{2,base}$ are consistent with zero at 2-σ in 70 % of the fits and at 3-σ for all of the fits. It is likely that $\Gamma_{0,base}$ is caused by residual gas, likely H_2, at our base or lowest pressure. Assuming H_2 gas with $K_{H_2} = 3.9(1) \times 10^{-9}$ cm^3/s [14], we derive $n_{base} = \Gamma_{0,base}/K_{H_2} = 6.9(1.5) \times 10^6$ cm^3/s, corresponding to base pressure $p_{base} = n_{base} k_B T = 2.8(6) \times$

10^{-8} Pa, in agreement with those extracted from decay curves measured at $n = 0$ in Ref. [15]. If the $\Gamma_{i,\mathrm{base}}$ for $i = 1$ and 2 are also caused by H_2 gas and if $\Xi(W,t) \ll 1$ for all t for both the residual gas and the species of interest, then we can show that $\Gamma_{1,\mathrm{base}} = a_{\mathrm{gl,base}} n_{\mathrm{base}}$ and $\Gamma_{2,\mathrm{base}} = b_{\mathrm{gl,base}} n_{\mathrm{base}}$. The corresponding fit values of a_{gl} and b_{gl} are consistent with the expected values of $a_{\mathrm{gl}} \approx 1.4 \times 10^{-7}$ cm^3/(s K) and $b_{\mathrm{gl}} \approx 8 \times 10^{-5}$ cm^3/(s K^2) for H_2, but also consistent with zero at 2-σ ($k = 2$) uncertainty.

Table III shows the comparison between the updated ^{87}Rb experimental values for K, a_{gl}, and b_{gl} and the corresponding original theoretical values of Ref. [14]. Generally the experimental values are now in better agreement with the theory. As with the results of Ref. [15], all numbers agree at two-standard deviations ($k = 2$) except K for ^{87}Rb-Ar, which agrees only at four-standard deviations ($k = 4$), and a_{gl} for ^{87}Rb-Kr, which agrees at three standard deviations ($k = 3$). Tables S3, S4, and S5 of the supplemental material [34] show a sample uncertainty budget for ^{87}Rb-Ar, the change in the values of K, a_{gl}, and b_{gl} from Ref. [15] to this work, and the current state of knowledge for values of K, respectively. The maximum relative change in K is -2.2 % for ^{87}Rb-Xe, as expected given that Xe results in the most glancing collisions.

V. CONCLUSION

We have developed a probabilistic and analytic model of glancing collisions in a CAVS. This model relaxes two assumptions that were implicit in previous literature: (1) that the sensor atoms cloud is at $T_{\mathrm{S}} = 0$, and (2) collisions that are not sufficient to eject a sensor atom from the trap also do not change the energy of the sensor atoms. While inspired by the recent semiclassical results of Ref. [12, 21], our model can use either semiclassical scattering theory [10–12, 21, 28] or fully quantum mechanical scattering theory [14, 16–19] as an input. We use our model to update the values of Ref. [15] based on a more complete description of the time evolution of the number of ultracold sensor atoms. We find that our relative adjustments for the theoretically predicted L for ^{7}Li-X are $\lesssim 0.6$ %. For ^{87}Rb-X, we find that our relative adjustments are as large as 2.2 % for our experimental, extrapolated zero-trap depth loss rate coefficients, K.

While specifically used to revisit the results of Ref. [15], the model presented here is applicable to a wide variety of experimental conditions including different types of traps, large W, and initial distributions of atoms, etc. For deep traps, the primary limitation is not the model presented here, but the knowledge of $P_{\mathrm{A}}(\Delta E)$, which our model uses as an input. While glancing collisions can never be fully avoided as the confining trap must have a non-zero depth, our model shows that ideally the trap depth should satisfy $\Xi(W,t) = |P_2(W) - [P_1(W)]^2| Knt \ll u(\eta_{\mathrm{S}})/\eta_{\mathrm{S}}$, where $u(\eta_{\mathrm{S}})/\eta_{\mathrm{S}}$ is the relative uncertainty in the measurement of the normalized sensor atom number. With this condition, the sensor-atom number decay measured at various times t remains exponential. Importantly, we note that a CAVS based on ^{7}Li is far less sensitive to the initial temperature of the cold atom cloud and the effects of glancing collisions than one based on ^{87}Rb. A CAVS based on ^{87}Rb can compensate for such complications, but requires ancillary measurements to achieve high levels of accuracy.

Appendix A: Collision kinematics and timescales

In this appendix, we briefly review the kinematics of collisions in the context of ultracold sensor atoms of mass m held in a trap with potential energy $U(\mathbf{r})$ at location $\mathbf{r}$ colliding with room-temperature background atoms or molecules. The minimum potential energy occurs at $\mathbf{r} = \mathbf{0}$ and $U(\mathbf{r} = \mathbf{0}) = 0$. Therefore, total energy $E = 0$ is the lowest energy of an atom in the trap, which occurs when it is at rest at $\mathbf{r} = \mathbf{0}$. Atoms with $E > 0$ execute classical orbits starting from position $\mathbf{r}$ and velocity $\mathbf{v}$ such that $E = m|\mathbf{v}|^2/2 + U(\mathbf{r})$ is conserved. For large $\mathbf{r}$, potential $U(\mathbf{r})$ approaches trap depth W from below along at least one direction $\mathbf{r}$. Typical timescales for orbits of atoms with magnetic moment μ in a quadrupole magnetic trap are $\tau_{\mathrm{orbit}} \sim \sqrt{2mk_{\mathrm{B}}T_{\mathrm{S}}/(\mu B')^2}$, where atom temperature $T_{\mathrm{S}} \ll W/k_{\mathrm{B}}$, $\mu \approx \mu_B$, μ_{B} is the Bohr magneton, and B' is the magnetic field gradient of the quadrupole trap. In our CAVSs, τ_{orbit} is of the order of 1 ms. If an atom is executing an orbit with $E > W$, it is not bound by the trap and is ejected.

The sensor atom and background particle do not move appreciably during the collision. This can be seen by noting that the duration of a collision is $\tau_{\mathrm{collision}} \sim \sqrt{\sigma_{\mathrm{eff}}}/\langle v \rangle$, where $\langle v \rangle$ is the mean velocity of the background gas atom or molecule at temperature T and $\sigma_{\mathrm{eff}} = K/\langle v \rangle \equiv \pi d_{\mathrm{eff}}^2$ is the effective cross section of the collision. That is, $\tau_{\mathrm{collision}}$ is related to the time it takes to traverse the effective diameter d_{eff} of the collision partners near room temperature. Given that $K \sim 10^{-9}$ cm^3/s and $\langle v \rangle \sim 10^4$ cm/s, we find that $\tau_{\mathrm{collision}} \sim 10$ ps $\ll \tau_{\mathrm{orbit}}$.

A consequence of the large difference in timescales $\tau_{\mathrm{collision}}$ and τ_{orbit} is that collisions occur at well-defined locations. Thus, the change in energy for a sensor atom with initial velocity $\mathbf{v}_{\mathrm{S}}$ and final velocity $\mathbf{v}_{\mathrm{S}} + \delta\mathbf{v}_{\mathrm{S}}$ colliding at location $\mathbf{r}$ with a background gas particle is

$$\begin{aligned} \Delta E &= U(\mathbf{r}) + \frac{1}{2}m(\mathbf{v}_{\mathrm{S}} + \delta\mathbf{v}_{\mathrm{S}})^2 - \left[U(\mathbf{r}) + \frac{1}{2}m\mathbf{v}_{\mathrm{S}}^2\right] \\ &= \frac{1}{2}m(\delta\mathbf{v}_{\mathrm{S}})^2 + m\mathbf{v}_{\mathrm{S}} \cdot \delta\mathbf{v}_{\mathrm{S}}\,. \end{aligned} \tag{A1}$$

For most collisions and even most glancing collisions $|\delta\mathbf{v}_{\mathrm{S}}| \gg |\mathbf{v}_{\mathrm{S}}|$ as $T_{\mathrm{S}} \ll T$ and $k_{\mathrm{B}}T_{\mathrm{S}} \ll W$, respectively. Furthermore, the bombardment from background gas particles is isotropic and thus the second term in Eq. (A1) is zero when averaged over all possible orientations of $\delta\mathbf{v}_{\mathrm{S}}$. We conclude that the "average" collision adds positive energy $\Delta E = m(\delta\mathbf{v}_{\mathrm{S}})^2/2$ to the sensor atom's orbit and that most glancing collisions with background gas particles, *i. e.* those with $\Delta E < W$, heat the sensor-atom cloud.

System	K (thr) (10^{-9}cm^3/s)	K (exp) (10^{-9}cm^3/s)	$E_n(K)$	a_{gl} (thr) (10^{-7}cm^3/[s K])	a_{gl} (exp) (10^{-7}cm^3/[s K])	$E_n(a_{gl})$	b_{gl} (thr) (10^{-5}cm^3/[s K^2])	b_{gl} (exp) (10^{-5}cm^3/[s K^2])	$E_n(b_{gl})$
^{87}Rb-^{4}He	2.37(3)	2.35(6)	−0.18	0.336(5)	−0.42(85)	0.44	0.067(3)	—	—
^{87}Rb-Ne	2.0(2)	2.21(5)	0.54	1.06(9)	1.2(7)	−0.09	0.59(3)	2.0(3.5)	−0.21
^{87}Rb-N_2	3.45(6)	3.56(8)	0.54	2.6(2)	1.9(1.4)	0.24	2.3577(7)	5.8(7.2)	−0.24
^{87}Rb-Ar	3.035(7)	3.29(5)	2.38	2.42(2)	2.6(8)	−0.11	2.19(2)	−2.4(3.9)	0.60
^{87}Rb-Kr	2.787(10)	2.80(4)	0.23	3.04(2)	1.8(5)	1.18	3.97(3)	3.8(2.5)	0.02
^{87}Rb-Xe	2.880(10)	2.87(6)	−0.08	4.11(5)	3.5(1.0)	0.30	7.1(1)	12.8(4.5)	−0.64

TABLE III. Theoretical [14] (thr) and updated experimental (exp) values for the loss rate coefficient K at zero trap depth, the first-order glancing rate coefficient a_{gl}, and the second-order glancing rate coefficient b_{gl} for various natural abundance gases colliding with ultracold ^{87}Rb atoms. Numbers in parentheses are one-standard-deviation, $k=1$ uncertainties. The degree of equivalence is $E_n(K) = (K_{exp} - K_{thr})/[2u(K_{exp} - K_{thr})]$ for K and likewise for a_{gl} and b_{gl}.

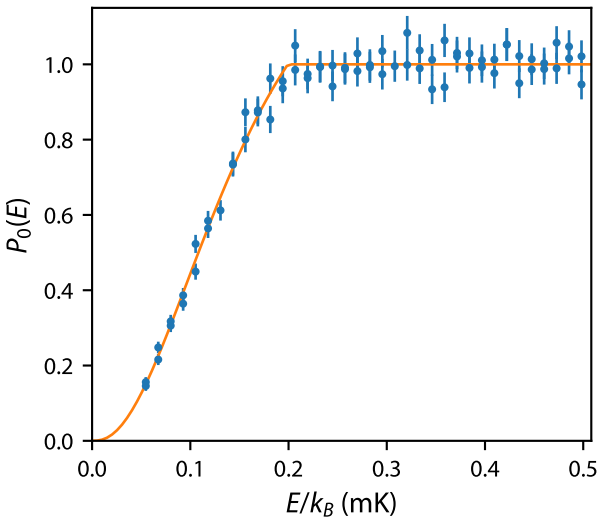

FIG. 2. Experimentally measured $P_0(T_S, E_c, E)$ with standard uncertainties (blue filled circles) for ^{87}Rb sensor atoms as a function of total energy E with cutoff energy $E_c = k_B \times 0.1993(2)$ mK. The solid orange curve is a fit of the data to Eq. (5) with temperature $T_S = 47(7)$ μK at a fixed value $\delta = 3/2$.

Appendix B: Experimental details and refined estimate of the temperature of ultracold ^{87}Rb samples

In this appendix, we first review the experimental details of Ref. 15 and update the temperature measurement T_S of the ultracold ^{87}Rb cloud. For the latter, we use a technique similar to that in Ref. [21].

Loss rate coefficients between various gases and ^{87}Rb were measured in the laboratory-scale cold-atom vacuum sensor (l-CAVS). As described in Refs. [13, 15], the l-CAVS combines a quadrupole magnetic trap and an "RF knife,", which applies radio-frequency magnetic fields to the atoms to induce spin-flip transitions at specific locations in a magnetic trap defined by the RF frequency ν_{RF} and local Zeeman shift in the trap. In Ref. [15], the RF knife was used to set cutoff energy E_c and trap depth W. To set E_c, a frequency ramp from $\nu_{RF}^{init} = 40$ MHz to $\nu_{RF}^{final} = 5$ MHz in 1 s removed atoms from the trap with total energy $E > E_c = h\nu_{RF}^{final}\{1 - 2mg/(\mu_B B')\} = k_B \times 0.1993(2)$ mK, where h is Planck's constant, m is the mass of ^{87}Rb, g is the predicted local gravitational acceleration from Ref. [35], and B' is the measured axial magnetic field gradient of the quadrupole trap. The uncertainty in E_c is limited by our knowledge of B'. Immediately after the ramp, the RF frequency was quickly (essentially instantaneously) changed to a constant, larger value to set trap depth W for the remainder of the measurement.

Here, we extend our use of the RF knife to measure the initial total-energy distribution $P_0(T_S, E_c, E)$ of ^{87}Rb atoms in the quadrupole magnetic trap as function of total energy E. We follow the procedure described above to prepare the cloud with $E_c = k_B \times 0.1993(2)$ mK and subsequently increase the RF frequency to 10 MHz leading to the smallest W used in Ref. [15]. In fact, $W = k_B \times 0.3986(4)$ mK. After holding the atoms in the trap for 10 s at this W, a hold time short compared to typical vacuum lifetimes of roughly 150 s and the typical Rb-Rb collisional thermalization time of roughly 30 s, frequency ν_{RF} is increased to 40 MHz and subsequently slowly decreased to a value between 100 kHz and 12.5 MHz, ejecting all ^{87}Rb atoms with energy $E > h\nu_{RF}(1 - 2mg/\mu_B B')$. Finally, we recapture the remaining sensor atoms into a MOT to count them to give $N(E)$ as in Ref. [15]. In this way, we measure the distribution $P_0(T_S, E_c, E) = N(E)/N_{init}$ between $E = k_B \times 3.986(4)$ μK and $k_B \times 0.4982(4)$ mK $\equiv E_{max}$, where N_{init} is the sensor atom number just before the frequency of the RF knife is slowly decreased from 40 MHz, which corresponds to $E = E_{init} \equiv k_B \times 1.5940(2)$ mK. Standard uncertainties in sensor atom number $N(E)$ are taken as in Ref. [15], with the $u(N) = \sqrt{(\sigma_N N^2) + \sigma_0^2}$, with $\sigma_N = 0.04$ and $\sigma_0 = 300$, yielding reduced χ_ν^2 values near unity and residuals that are independent of E. In practice, as $E_{max} < E_{init}$ atom number N_{init} is taken as an adjusted constant.

The results of the measurement of $N(E)$ and thus $P_0(T_S, E_c, E)$ as a function of E for $E_c = k_B \times 0.1993(2)$ mK are shown in Fig. 2. For $E > E_c$, $P_0(T_S, E_c, E)$ is constant, showing both the effectiveness of the initial sweep of the RF knife to remove "hot" sensor atoms and the lack of a significant number of Rb-Rb rethermalizing collisions during the 10 s hold time. For the present experiment, the RF antenna is less effective at removing ^{87}Rb atoms with $E/k_B \lesssim 0.05$ mK, so no data are shown in that region. A fit with T_S, δ, and N_{init} as adjusted constants yields $T_S = 59(8)$ μK and $\delta = 1.13(19)$,

which includes at 2-σ our expected value of $\delta = 3/2$. A second fit, indistinguishable in Fig. 2, with a fixed and physically motivated value of $\delta = 3/2$, yields $T_S = 47(7)$ μK. In an attempt to account for systematic effects, we take as a conservative estimate for T_S the weighted mean of the two estimated temperatures assuming a standard uncertainty given by the temperature difference, which gives $T_S = 53(12)$ μK.

ACKNOWLEDGEMENTS

The authors thank K. Madison, J. Booth, and A. Deshmukh for useful discussions; K. Madison and R. Krems for organizing the workshop that helped to elucidate the physics, and P.J. Egan and B. Reschovsky for a thorough reading of the manuscript.

AUTHOR DECLARATIONS

Conflicts of Interest

D.S.B., J.A.F., J.S., and S.P.E. have U.S. patent 11,291,103 issued. D.S.B. and S.P.E. have filed U.S. provisional patent 63/338,047.

DATA AVAILABILITY

The data that support the findings of this study are available from the corresponding author upon reasonable request.

[1] J. E. Bjorkholm, Collision-limited lifetimes of atom traps, Phys. Rev. A **38**, 1599 (1988).
[2] D. E. Fagnan, J. Wang, C. Zhu, P. Djuricanin, B. G. Klappauf, J. L. Booth, and K. W. Madison, Observation of quantum diffractive collisions using shallow atomic traps, Phys. Rev. A **80**, 022712 (2009).
[3] J. Booth, D. E. Fagnan, B. G. Klappauf, K. W. Madison, and J. Wang, Method and device for accurately measuring the incident flux of ambient particles in a high or ultra-high vacuum environment (2011), US Patent 8,803,072.
[4] T. Arpornthip, C. A. Sackett, and K. J. Hughes, Vacuum-pressure measurement using a magneto-optical trap, Phys. Rev. A **85**, 033420 (2012).
[5] J.-P. Yuan, Z.-H. Ji, Y.-T. Zhao, X.-F. Chang, L.-T. Xiao, and S.-T. Jia, Simple, reliable, and nondestructive method for the measurement of vacuum pressure without specialized equipment., Appl. Opt. **52**, 6195 (2013).
[6] R. W. G. Moore, L. A. Lee, E. A. Findlay, L. Torralbo-Campo, G. D. Bruce, and D. Cassettari, Measurement of vacuum pressure with a magneto-optical trap: A pressure-rise method, Rev. Sci. Instrum. **86**, 093108 (2015).
[7] V. B. Makhalov, K. A. Martiyanov, and A. V. Turlapov, Primary vacuometer based on an ultracold gas in a shallow optical dipole trap, Metrologia **53**, 1287 (2016).
[8] J. Scherschligt, J. A. Fedchak, D. S. Barker, S. Eckel, N. Klimov, C. Makrides, and E. Tiesinga, Development of a new UHV/XHV pressure standard (cold atom vacuum standard), Metrologia **54**, S125 (2017).
[9] S. Eckel, D. S. Barker, J. A. Fedchak, N. N. Klimov, E. Norrgard, J. Scherschligt, C. Makrides, and E. Tiesinga, Challenges to miniaturizing cold atom technology for deployable vacuum metrology, Metrologia **55**, S182 (2018).
[10] J. L. Booth, P. Shen, R. V. Krems, and K. W. Madison, Universality of quantum diffractive collisions and the quantum pressure standard, New J. Phys. **21**, 102001 (2019).
[11] P. Shen, K. W. Madison, and J. L. Booth, Realization of a universal quantum pressure standard, Metrologia **57**, 025015 (2020).
[12] P. Shen, K. W. Madison, and J. L. Booth, Refining the cold atom pressure standard, Metrologia **58**, 022101 (2021).
[13] D. S. Barker, B. P. Acharya, J. A. Fedchak, N. N. Klimov, E. B. Norrgard, J. Scherschligt, E. Tiesinga, and S. P. Eckel, Precise quantum measurement of vacuum with cold atoms, Rev. Sci. Instrum. **93**, 121101 (2022).
[14] J. Kłos and E. Tiesinga, Elastic and glancing-angle rate coefficients for heating of ultracold Li and Rb atoms by collisions with room-temperature noble gases, H_2, and N_2, The Journal of Chemical Physics **158**, 014308 (2023).
[15] D. S. Barker, J. A. Fedchak, J. Kłos, J. Scherschligt, A. A. Sheikh, E. Tiesinga, and S. P. Eckel, Accurate measurement of the loss rate of cold atoms due to background gas collisions for the quantum-based cold atom vacuum standard, AVS Quantum Science **5**, 035001 (2023).
[16] C. Makrides, D. S. Barker, J. A. Fedchak, J. Scherschligt, S. Eckel, and E. Tiesinga, Elastic rate coefficients for Li+H_2 collisions in the calibration of a cold-atom vacuum standard, Phys. Rev. A **99**, 042704 (2019).
[17] C. Makrides, D. S. Barker, J. A. Fedchak, J. Scherschligt, S. Eckel, and E. Tiesinga, Collisions of room-temperature helium with ultracold lithium and the van der Waals bound state of HeLi, Phys. Rev. A **101**, 012702 (2020).
[18] C. Makrides, D. S. Barker, J. A. Fedchak, J. Scherschligt, S. Eckel, and E. Tiesinga, Erratum: Collisions of room-temperature helium with ultracold lithium and the van der Waals bound state of HeLi, Phys. Rev. A **105**, 029902 (2022).
[19] C. Makrides, D. S. Barker, J. A. Fedchak, J. Scherschligt, S. Eckel, and E. Tiesinga, Erratum: Elastic rate coefficients for Li+H_2 collisions in the calibration of a cold-atom vacuum standard, Phys. Rev. A **105**, 039903 (2022).
[20] Because the expressions for $P_A(\Delta E)$ that appear in the literature were derived using assumptions (1) and (2), these functions are actually $P_A(W)$. Fundamentally, however, they are expressions for the probability of a collision adding kinetic energy of at least ΔE to the sensor atom.
[21] R. A. Stewart, P. Shen, J. L. Booth, and K. W. Madison, Measurement of Rb-Rb van der Waals coefficient via quantum diffractive universality, Phys. Rev. A **106**, 052812 (2022).
[22] A. Deshmukh, R. A. Stewart, P. Shen, J. L. Booth, and K. W. Madison, Trapped-particle evolution driven by residual gas collisions, Phys. Rev. A **109**, 032818 (2024).
[23] C. Grinstead and J. Snell, *Introduction to Probability* (American Mathematical Society, 2012).
[24] V. Bagnato, D. E. Pritchard, and D. Kleppner, Bose-Einstein condensation in an external potential, Phys. Rev. A **35**, 4354

(1987).
[25] O. J. Luiten, M. W. Reynolds, and J. T. M. Walraven, Kinetic theory of the evaporative cooling of a trapped gas, Phys. Rev. A **53**, 381 (1996).
[26] C. Pethick and H. Smith, *Bose-Einstein Condensation in Dilute Gases* (Cambridge University Press, 2002).
[27] L. H. Ehinger, B. P. Acharya, D. S. Barker, J. A. Fedchak, J. Scherschligt, E. Tiesinga, and S. Eckel, Comparison of two multiplexed portable cold-atom vacuum standards, AVS Quantum Sci. **4**, 034403 (2022).
[28] P. Shen, E. Frieling, K. R. Herperger, D. Uhland, R. A. Stewart, A. Deshmukh, R. V. Krems, J. L. Booth, and K. W. Madison, Cross-calibration of atomic pressure sensors and deviation from quantum diffractive collision universality for light particles, New J. Phys. **25**, 053018 (2023).
[29] S. Bali, K. M. O'Hara, M. E. Gehm, S. R. Granade, and J. E. Thomas, Quantum-diffractive background gas collisions in atom-trap heating and loss, Phys. Rev. A **60**, R29 (1999).
[30] DLMF, *NIST Digital Library of Mathematical Functions*, https://dlmf.nist.gov/, Release 1.2.1 of 2024-06-15, f. W. J. Olver, A. B. Olde Daalhuis, D. W. Lozier, B. I. Schneider, R. F. Boisvert, C. W. Clark, B. R. Miller, B. V. Saunders, H. S. Cohl, and M. A. McClain, eds.
[31] Note that in Ref. [15] for practical reasons, $\eta_S(t)$ was the ratio of the measured atom number in the magnetic trap after time t to the atom number in the magneto-optical trap (MOT) just before transfer into the magnetic trap.
[32] The simulations are stable against changes in Δt, provided that $Kn\Delta t \ll 1$.
[33] D. Barker, E. Norrgard, N. Klimov, J. Fedchak, J. Scherschligt, and S. Eckel, Single-beam Zeeman slower and magneto-optical trap using a nanofabricated grating, Phys. Rev. Applied **11**, 064023 (2019).
[34] See Supplemental Material at [URL will be inserted by publisher] for tables showing the shift in the experimental values, updated uncertainty budgets, and updated comparison with other literature values.
[35] N. Oceanic and A. Administration, Surface gravity prediction, https://www.ngs.noaa.gov/cgi-bin/grav_pdx.prl.